

Implicit Methods with Reduced Memory for Thermal Radiative Transfer

Dmitriy Y. Anistratov^b, Joseph M. Coale^c

^a*Department of Nuclear Engineering, North Carolina State University Raleigh, NC*

^b*anistratov@ncsu.edu*

^c*jmcoble@ncsu.edu*

Abstract

This paper presents approximation methods for time-dependent thermal radiative transfer problems in high energy density physics. It is based on the multilevel quasidiffusion method defined by the high-order radiative transfer equation (RTE) and the low-order quasidiffusion (aka VEF) equations for the moments of the specific intensity. A large part of data storage in TRT problems between time steps is determined by the dimensionality of grid functions of the radiation intensity. The approximate implicit methods with reduced memory for the time-dependent Boltzmann equation are applied to the high-order RTE, discretized in time with the backward Euler (BE) scheme. The high-dimensional intensity from the previous time level in the BE scheme is approximated by means of the low-rank proper orthogonal decomposition (POD). Another version of the presented method applies the POD to the remainder term of P_2 expansion of the intensity. The accuracy of the solution of the approximate implicit methods depends of the rank of the POD. The proposed methods enable one to reduce storage requirements in time dependent problems. Numerical results of a Fleck-Cummings TRT test problem are presented.

Keywords: high-energy density physics, Boltzmann equation, radiative transfer, implicit schemes, memory reduction, proper orthogonal decomposition, multilevel methods

1. Introduction

We consider the thermal radiative transfer (TRT) problem in 1D slab geometry that is defined by the time-dependent radiative transfer equation (RTE)

$$\frac{1}{c} \frac{\partial I_g}{\partial t}(x, \mu, t) + \mu \frac{\partial I_g}{\partial x}(x, \mu, t) + \kappa_g(T) I_g(x, \mu, t) = \kappa_g(T) B_g(T), \quad (1)$$

$$x \in [0, X], \quad \mu \in [-1, 1], \quad g \in \mathbb{N}(G), \quad t \geq t_0,$$

$$I_g|_{\mu>0, x=0} = I_g^{in+}, \quad I_g|_{\mu<0, x=X} = I_g^{in-}, \quad I_g|_{t=t_0} = I_g^0, \quad (2)$$

and the material energy balance (MEB) equation

$$\frac{\partial \varepsilon(T)}{\partial t} = \sum_{g=1}^G \kappa_g(T) \left(\int_{-1}^1 I_g(x, \mu, t) d\mu - 2B_g(T) \right), \quad T|_{t=t_0} = T_0, \quad (3)$$

where I_g is the group specific photon intensity; x is the spatial position; μ is the direction cosine of particle motion; g is the index of photon frequency group; $\mathbb{N}(G) = \{1, \dots, G\}$; t is time; κ_g is the group opacity; T is the material temperature; ε is the material energy density; B_g is the group Planck black-body distribution function.

The solution of the multigroup RTE in general geometry depends on 7 independent variables. Temporal discretization schemes for the RTE involve the discrete solution at the previous time level. This requires storing in memory 6-dimensional grid functions that approximate the transport solution on a given mesh in the phase space. There are different approaches for developing approximate methods for time-dependent transport problems that reduce memory requirements [1, 2, 3, 4, 5]. The α -approximation of the intensity in time reduces the RTE to a transport equation of steady-state form with a modified opacity [1]. This approximation assumes that the intensity varies exponentially over each time interval. The approximate rate of change in time can be obtained by means of the solution of low-order moment equations. As such, the α -approximation rids one of the need to store the high-dimensional solution from the previous time level [1]. This approximation method for the time-dependent RTE demonstrated good accuracy in TRT problems [6, 7]. Analysis showed that there are some limitations for the RTE in the α -approximation [4].

Recently, approximate implicit methods with reduced memory for the time-dependent Boltzmann transport equation have been proposed [5]. They use the modified backward Euler (MBE) time integration scheme that applies the proper orthogonal decomposition (POD) of the transport solution from the previous time step to compress the data and reduce memory requirements [8, 9, 10]. The accuracy of the method depends on the order of the low-rank POD of the discrete transport solution. The error decreases as rank increases. In this paper, we apply the MBE scheme within the framework of the multilevel quasidiffusion (MLQD) method for solving TRT problems [6, 11, 12].

The remainder of the paper is organized as follows. In Sec. 2, the MLQD method with approximate implicit scheme is formulated. In Sec. 3, we present different approximations of the specific intensity by means of the POD. The numerical results are presented in Sec. 4. We conclude with a discussion in Sec. 5.

2. The MLQD Method with Approximate Implicit Scheme for the High-Order Problem

2.1. MLQD Equations and Discretization

The MLQD method is defined by a system of equations consisting of

1. the multigroup high-order RTE (Eq. (1))

$$\frac{1}{c} \frac{\partial I_g}{\partial t} + \mu \frac{\partial I_g}{\partial x} + \kappa_g I_g = \kappa_g B_g, \quad (4)$$

2. the multigroup low-order quasidiffusion (aka VEF) equations for the group radiation energy density and flux [11, 13]

$$\frac{\partial E_g}{\partial t} + \frac{\partial F_g}{\partial x} + c \kappa_g E_g = 2 \kappa_g B_g, \quad (5a)$$

$$\frac{1}{c} \frac{\partial F_g}{\partial t} + c \frac{\partial(f_g E_g)}{\partial x} + \kappa_g F_g = 0, \quad (5b)$$

where

$$f_g = \frac{\int_{-1}^1 \mu^2 I_g d\mu}{\int_{-1}^1 I_g d\mu} \quad (5c)$$

is the group QD (Eddington) factor,

- the effective grey low-order quasidiffusion (LOQD) equations for the total radiation energy density and fluxes

$$\frac{\partial E}{\partial t} + \frac{\partial F}{\partial x} + c \bar{\kappa}_E E = c \bar{\kappa}_B a_R T^4, \quad (6a)$$

$$\frac{1}{c} \frac{\partial F}{\partial t} + c \frac{\partial(\bar{f}_E E)}{\partial x} + \bar{\kappa}_{|F|} F + \bar{\eta} E = 0, \quad (6b)$$

where the spectrum averaged opacities and factors are defined by

$$\bar{\alpha}_H = \frac{\sum_{g=1}^G \alpha_g H_g}{\sum_{g=1}^G H_g}, \quad \bar{\eta} = \frac{\sum_{g=1}^G (\kappa_g - \bar{\kappa}_{|F|}) F_g}{\sum_{g=1}^G E_g}, \quad (7)$$

- the MEB equation (3) in grey form

$$\frac{\partial \varepsilon(T)}{\partial t} = c (\bar{\kappa}_E E - \bar{\kappa}_B a_R T^4). \quad (8)$$

We discretize the equations of the MLQD method by the backward Euler (BE) time integration scheme. This yields the semi-discrete RTE at the n -th time level given by

$$\frac{1}{c \Delta t^n} (I_g^n - I_g^{n-1}) + \mu \frac{\partial I_g^n}{\partial x} + \kappa_g^n I_g^n = Q_g^n, \quad (9)$$

where $\Delta t^n = t^n - t^{n-1}$ is the n -th time step, $Q_g^n = \kappa_g(T^n) B_g(T^n)$. The high-order equation (9) is discretized in space by the step characteristic (SC) scheme. The multigroup LOQD equations discretized in time by the BE scheme have the following form:

$$\frac{1}{\Delta t^n} (E_g^n - E_g^{n-1}) + \frac{\partial F_g^n}{\partial x} + c \kappa_g^n E_g^n = 2Q_g^n, \quad (10a)$$

$$\frac{1}{c \Delta t^n} (F_g^n - F_g^{n-1}) + c \frac{\partial(f_g^n E_g^n)}{\partial x} + \kappa_g^n F_g^n = 0, \quad (10b)$$

$$f_g^n = \frac{\int_{-1}^1 \mu^2 I_g^n d\mu}{\int_{-1}^1 I_g^n d\mu}. \quad (11)$$

The grey LOQD and MEB equations approximated with the BE scheme are defined by

$$\frac{1}{\Delta t^n} (E^n - E^{n-1}) + \frac{\partial F^n}{\partial x} + c \bar{\kappa}_E^n E^n = c \bar{\kappa}_B^n a_R (T^n)^4, \quad (12a)$$

$$\frac{1}{c\Delta t^n}(F^n - F^{n-1}) + c\frac{\partial(\bar{f}_E^n E^n)}{\partial x} + \bar{\kappa}_{[F]}^n F^n + \bar{\eta}^n E^n = 0. \quad (12b)$$

$$\frac{1}{\Delta t^n}(\varepsilon(T^n) - \varepsilon(T^{n-1})) = c(\bar{\kappa}_E^n E^n - \bar{\kappa}_B^n a_R(T^n)^4). \quad (13)$$

The multigroup LOQD equations are discretized in space by a second-order finite volume (FV) method. The spatial discretization of the grey LOQD equations is algebraically consistent with the discretized multigroup LOQD equations [7]. We refer to the described method as the MLQD method with BE-SC scheme.

2.2. Approximate Implicit Method for the RTE

In the approximate implicit scheme, the multigroup RTE (4) is discretized by the MBE time integration scheme given by [5]

$$\frac{1}{c\Delta t^n}(I_g^n - \hat{I}_g^{n-1}) + \mu \frac{\partial I_g^n}{\partial x} + \kappa_g^n I_g^n = Q_g^n, \quad (14)$$

where the grid functions of group intensity \hat{I}_g^{n-1} are approximated by the low-rank POD of the solution I_g^{n-1} computed at the time step $n - 1$. The SC scheme for the high-order equation (14) is formulated for the cell-edge ($I_{gmj+1/2}^n$) and cell-average (I_{gmj}^n) angular fluxes by means of the detailed particle balance equation and weighted auxiliary relation

$$\frac{\Delta x_j}{c\Delta t^n}(I_{gmj}^n - \hat{I}_{gmj}^{n-1}) + \mu_m(I_{gmj+1/2}^n - I_{gmj-1/2}^n) + \kappa_{gj}^n I_{gmj}^n \Delta x_j = Q_{gj}^n \Delta x_j, \quad (15a)$$

$$I_{gmj}^n = \gamma_{gmj}^n I_{gmj-1/2}^n + (1 - \gamma_{gmj}^n) I_{gmj+1/2}^n, \quad (15b)$$

$$\gamma_{gmj}^n = \frac{1}{\tau_{gmj}^n} - \frac{1}{e^{\tau_{gmj}^n} - 1}, \quad \tau_{gmj}^n = \frac{1}{\mu_m}(\kappa_{gj}^n + (c\Delta t^n)^{-1})\Delta x_j, \quad (15c)$$

where $m \in \mathbb{N}(M)$ is the index of angular direction, $j \in \mathbb{N}(J)$ is the index of the spatial interval, Δx_j is the width of the j -th cell. We refer to the discretized RTE (15) as the MBE-SC scheme.

3. Approximation of the Specific Intensity

3.1. POD of the Intensity

The MBE-SC scheme (Eqs. (15)) needs to store the cell-average intensity I_{gmj}^n . In each photon frequency group, it is a 2D discrete grid function of j and m . We interpret it in a matrix form defined by $A_I = [\mathbf{I}_1 \dots \mathbf{I}_M]$ ($A_I \in \mathbb{R}^{J \times M}$), where the columns are given by $\mathbf{I}_m = [I_{m1} \dots I_{mJ}]^T$ ($\mathbf{I}_m \in \mathbb{R}^J$). Here we omitted group and time indices for the sake of brevity. We approximate the grid function of the group cell-average intensity by the low-rank POD [9, 10]. The reduced singular value decomposition (SVD) of A_I has the form:

$$A_I = U_I \Lambda_I V_I^T. \quad (16)$$

$\Lambda_I = \text{diag}(\lambda_1 \dots \lambda_d) \in \mathbb{R}^{d \times d}$ is the diagonal matrix of singular values, where

$$d = \min(J, M) \quad (17)$$

is the rank of A_I . $U_I = [\mathbf{u}_1 \dots \mathbf{u}_d]$ and $V_I = [\mathbf{v}_1 \dots \mathbf{v}_d]$ are the matrices of left and right singular vectors, respectively, where $\mathbf{u}_\ell \in \mathbb{R}^J$ and $\mathbf{v}_\ell \in \mathbb{R}^M$. The approximate group intensity $\hat{\mathbf{I}}_m = [\hat{I}_{m1} \dots \hat{I}_{mJ}]^T$ is defined by the low-rank POD of A_I given by

$$\hat{A}_I^r = \sum_{\ell=1}^r \lambda_\ell \mathbf{u}_\ell \otimes (\mathbf{v}_\ell)^T, \quad r < d, \quad \text{where} \quad \hat{A}_I = [\hat{\mathbf{I}}_1 \dots \hat{\mathbf{I}}_M]. \quad (18)$$

This is the optimal approximation of the matrix A_I in the 2-norm [10, 14]. The low-rank approximation (18) requires storage of the first r singular values and associated left and right singular vectors. Thus, this approximation leads to memory allocation of a data set with the number of elements $r(J + M + 1)$ in each group. The rank can be chosen according to various criteria.

3.2. POD of the Remainder Term

We cast the intensity as its P_2 approximation and the remainder term defined by

$$\Delta I_{mj} = I_{mj} - \frac{1}{2} \left(\tilde{\phi}_j + 3\mu_m \tilde{F}_j + \frac{5}{4} (3\mu_m^2 - 1) (3f_j - 1) \tilde{\phi}_j \right), \quad (19)$$

where the P_2 expansion coefficients are calculated by the solution of the high-order RTE, namely,

$$\tilde{\phi}_j = \sum_{m=1}^M I_{mj} w_m, \quad \tilde{F}_j = \sum_{m=1}^M \mu_m I_{mj} w_m, \quad f_j = \frac{\sum_{m=1}^M \mu_m^2 I_{mj} w_m}{\sum_{m=1}^M I_{mj} w_m}. \quad (20)$$

The discrete 2D function ΔI_{mj} is treated as a matrix defined by $\Delta A_I = [\Delta \mathbf{I}_1 \dots \Delta \mathbf{I}_M]$, where $\Delta \mathbf{I}_m = [\Delta I_{m1} \dots \Delta I_{mJ}]^T$. Its POD is given by

$$\Delta A_I = U'_I \Lambda'_I (V'_I)^T. \quad (21)$$

where $\Lambda'_I = \text{diag}(\lambda'_1 \dots \lambda'_d) \in \mathbb{R}^{d \times d}$, $U'_I = [\mathbf{u}'_1 \dots \mathbf{u}'_d]$, $V'_I = [\mathbf{v}'_1 \dots \mathbf{v}'_d]$, $\mathbf{u}'_\ell \in \mathbb{R}^J$, and $\mathbf{v}'_\ell \in \mathbb{R}^M$. We apply the low-rank POD

$$\Delta \hat{A}_I^r = [\Delta \hat{\mathbf{I}}_1 \dots \Delta \hat{\mathbf{I}}_M] = \sum_{k=1}^r \lambda'_k \mathbf{u}'_k \otimes (\mathbf{v}'_k)^T, \quad r < d, \quad \Delta \hat{\mathbf{I}}_m = [\Delta \hat{I}_{m1}, \dots, \Delta \hat{I}_{mJ}]^T \quad (22)$$

to define approximate intensities as the sum of its P_2 approximation and the POD of the remainder term

$$\hat{I}_{mj} = \frac{1}{2} \left(\tilde{\phi}_j + 3\mu_m \tilde{F}_j + \frac{5}{4} (3\mu_m^2 - 1) (3f_j^n - 1) \tilde{\phi}_j \right) + \Delta \hat{I}_{mj}. \quad (23)$$

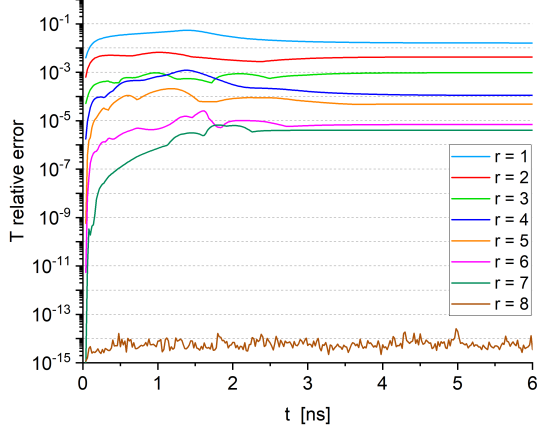
This approximation needs to store in memory $r(J + M + 1) + 2J$ elements that includes (i) $r(J + M + 1)$ elements for the remainder term and (ii) $2J$ elements for vectors of two angular moments $\tilde{\phi}$ and \tilde{F} .

4. Numerical Results

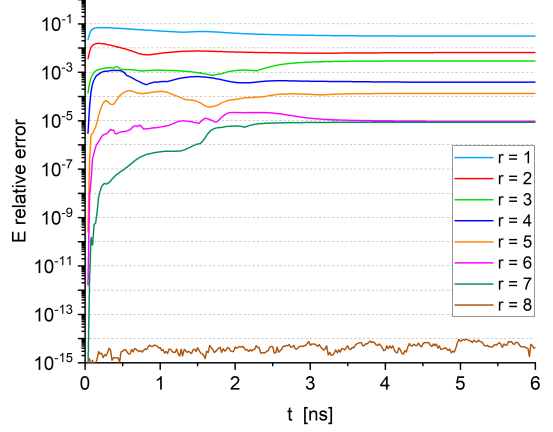
We present numerical results of the Fleck-Cummings (F-C) test [15]. The spatial domain ($0 \leq x \leq 6$) contains one material. The spectral opacity of the material is given by $\kappa_\nu = \frac{27}{(h\nu)^3} (1 - e^{-\frac{h\nu}{kT}})$. There is incoming radiation with black-body spectrum B_ν at temperature $kT_{in} = 1$ keV at the left boundary. The right boundary is vacuum. The initial temperature of the slab is $kT_0 = 1$ eV. At $t = 0$ the radiation intensity in the slab has the black-body spectrum at T_0 . The material energy density is $\varepsilon = c_\nu T$, where $c_\nu = 0.5917 a_R T_{in}^3$. The problem is solved over the time interval $0 \leq t \leq 6$ ns. The time step size is $\Delta t = 2 \times 10^{-2}$ ns. The uniform spatial mesh consists of $J = 100$ cells. The angular mesh has 8 discrete directions ($M = 8$). The double S_4 Gauss-Legendre quadrature set is used. We define $G = 17$ energy groups. The parameters of convergence criteria for temperature and energy density are $\epsilon_T = \epsilon_E = 10^{-12}$, respectively.

The discrete solution of the MLQD method with the MBE-SC scheme, namely, the total radiation energy density E_h^r and temperature T_h^r of the approximate implicit method with the rank r POD is compared to the discrete solution T_h and E_h of the MLQD method with the BE-SC scheme on the corresponding grid in the phase space and time. The numerical results of the method with the POD of the intensity of the rank r in all groups are presented in Figure 1. The plots show the relative error in reproducing the discrete solution in ∞ -norm, namely, $\frac{\|T_h - T_h^r\|_\infty}{\|T_h\|_\infty}$ and $\frac{\|E_h - E_h^r\|_\infty}{\|E_h\|_\infty}$ for the complete range of r . The results obtained with the MBE-SC scheme using the POD of the rank r of the remainder term in each group are shown in Figure 2. In this test, the full rank d (Eq. (17)) equals 8. The results with the full-rank POD ($r = 8$) of both methods illustrate that they accurately reproduce the discrete solution of the MLQD method with the SC scheme on the given grid as expected. In case $r = 5, 6, 7$ the solution of the method with the POD of the remainder term has very small error. This is due to explicit accounting for the first three Legendre moments of the intensity (Eq. (23)). The singular eigenvalues λ_ℓ for $\ell = 5, 6, 7$ in groups are very small. In this test problem, the method with POD of the remainder term is predominantly more accurate than to the method with POD of the intensity for the given rank r . However, it uses more data for the rank r . Figure 3 shows the ratio between errors of the method with the POD of the remainder term (POD-RT) and the one with the POD of the intensity (POD-I).

The gains in memory allocation depend on both the number of spatial cells J and angular directions M and hence are problem specific. For the phase-space grid used in the test, the size of the data set stored by this MLQD method with the RTE discretized the BE-SC scheme at the end of each time step is $D = G(J \times M + 2 \times J + 1) + 2 \times J + 1 = 17218$. This includes the data for (i) the multigroup RTE, (ii) the multigroup and grey LOQD equations, and (iii) the MEB equation. Table 1 shows the percentage reduction of required data storage sizes of the MLQD method with each of the two versions of the MBE-SC scheme compared to that of the MLQD method with the BE-SC scheme. Negative values indicate an increase in storage compared to the BE-SC scheme. In this test, the method with POD of intensities shows gains in memory for all ranks, i.e. $r = 1, \dots, 7$. The method with POD of the remainder term reduces memory allocation for $r = 1, \dots, 5$.

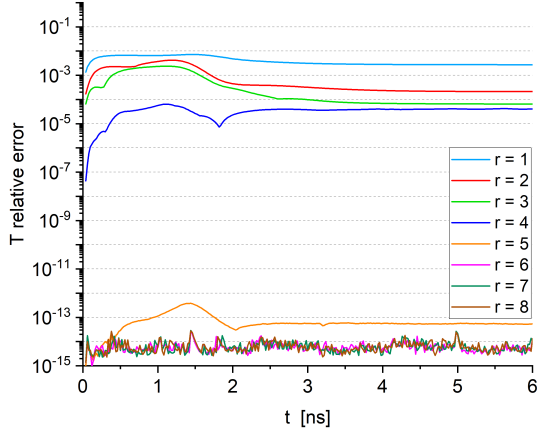


(a) $\frac{\|T_h - T_h^r\|_\infty}{\|T_h\|_\infty}$.

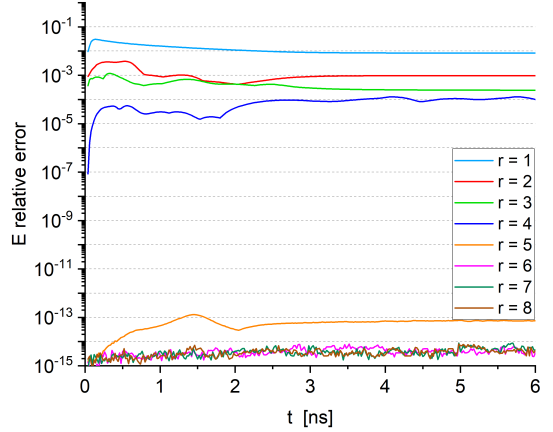


(b) $\frac{\|E_h - E_h^r\|_\infty}{\|E_h\|_\infty}$.

Figure 1: Relative error in ∞ -norm of the solution of the MLQD method with the MBE-SC scheme and POD of the intensity compared to the discrete solution on the corresponding grid in phase space and time.



(a) $\frac{\|T_h - T_h^r\|_\infty}{\|T_h\|_\infty}$.



(b) $\frac{\|E_h - E_h^r\|_\infty}{\|E_h\|_\infty}$.

Figure 2: Relative error in ∞ -norm of the solution of the MLQD method with the MBE-SC scheme and POD of the remainder term compared to the discrete solution on the corresponding grid in phase space and time.

Figures 4 and 5 present the results of spatial mesh refinement for the fixed time step size $\Delta t = 2 \times 10^{-2}$ ns. They show the relative error of E in ∞ -norm for uniform meshes with $\Delta x = 0.24, 0.12, 0.06, 0.03$ cm. The number of degrees of freedom of the discrete intensity increases with refinement of spatial mesh. The results show that the change in the relative error decreases with refinement. The factor of change on fine meshes approaches one. This

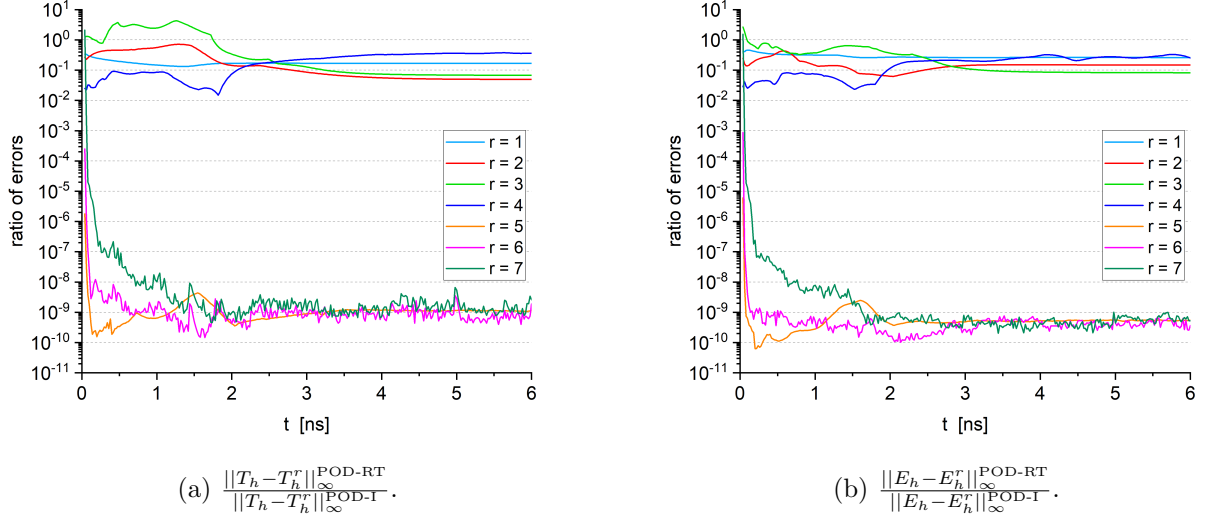


Figure 3: The error of the method with POD of the remainder term (POD-RT) over the error of the method with POD of intensity (POD-I).

Table 1: Reduction [%] in memory storage of previous step data of the MLQD method with the MBE-SC scheme ($J=100$, $M=8$).

Rank (r)	1	2	3	4	5	6	7
POD-I	68.2	57.5	46.7	35.9	25.2	14.4	3.7
POD-RT	48.5	37.7	27.0	16.2	5.4	-5.3	-16.1

indicates that the error due to low-rank POD of data representing intensities tends to a limit as $\Delta x \rightarrow 0$ for the fixed time step Δt . Figures 6 and 7 present the relative error of E in ∞ -norm for the numerical solution computed with refined time steps ($\Delta t = 4 \times 10^{-2}$, 2×10^{-2} , 10^{-2} , 5×10^{-3} ns) on the spatial mesh with $\Delta x = 6 \times 10^{-2}$ cm. These results show increase in the relative error in reproducing the discrete solution on the given grids. More analysis is needed to study properties of the methods.

5. Conclusions

This paper presented implicit methods with approximate time evolution operator in the high-order Boltzmann equation and reduced memory for TRT problems. The obtained results showed that the proposed methods reproduce the numerical solution of the underlying discretization method on the given phase-space grid with various degrees of accuracy while reducing storage of data between time steps. The accuracy depends on the rank of the POD of the data representing intensity from the previous time level. It is possible to achieve accuracy that is good for practical routine simulations and significantly reduce memory usage. There are extra computational costs due to calculations of the POD of intensities.

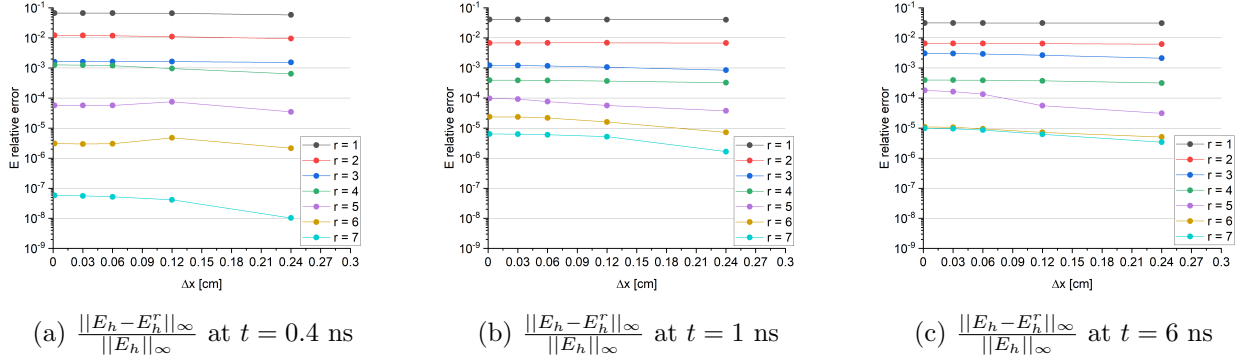


Figure 4: Results of refinement of spatial mesh for the MLQD method with the MBE-SC scheme and POD of the intensity for $\Delta t = 2 \times 10^{-2}$.

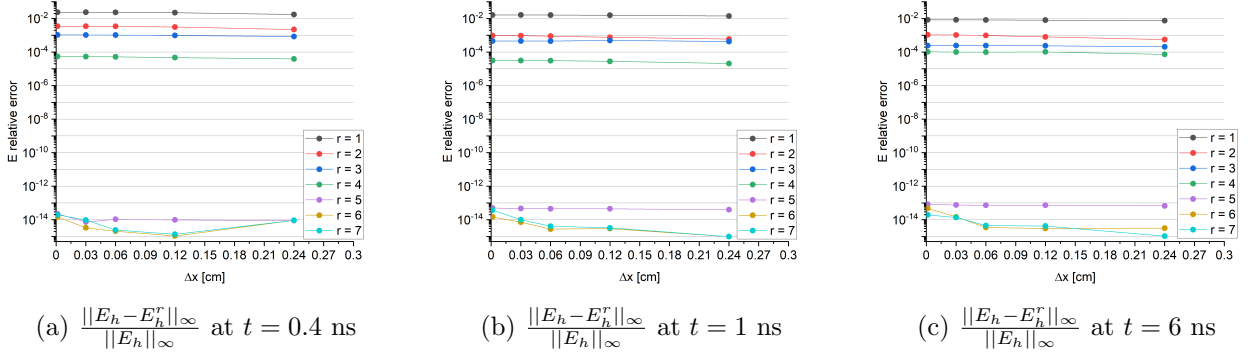
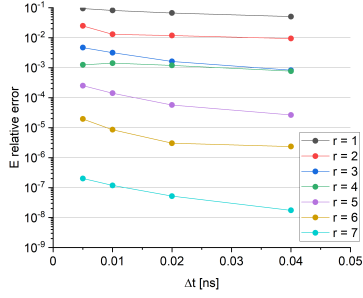


Figure 5: Results of spatial mesh refinement for the MLQD method with the MBE-SC scheme and POD of the remainder term for $\Delta t = 2 \times 10^{-2}$ ns.

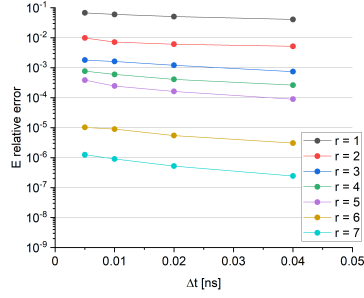
The proposed approximate implicit methods are intended for computer architectures on which one can take advantage of extra computations for reduction of memory storage. The proposed approach can be applied to various time integration methods and different kind of transport problems.

Acknowledgements

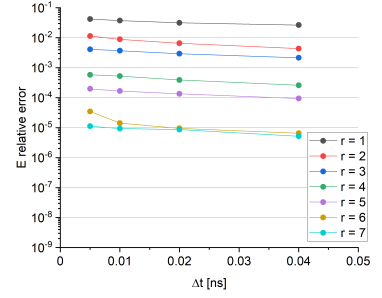
This research project is funded by the Department of Defense, Defense Threat Reduction Agency, grant number HDTRA1-18-1-0042. The content of the information does not necessarily reflect the position or the policy of the federal government, and no official endorsement should be inferred.



(a) $\frac{\|E_h - E_h^r\|_\infty}{\|E_h\|_\infty}$ at $t = 0.4$ ns

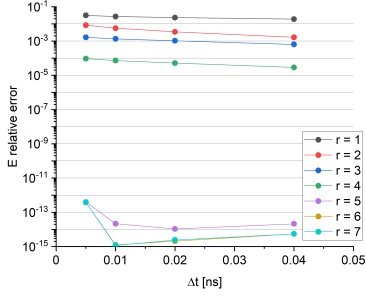


(b) $\frac{\|E_h - E_h^r\|_\infty}{\|E_h\|_\infty}$ at $t = 1$ ns

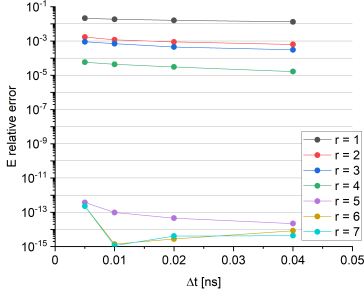


(c) $\frac{\|E_h - E_h^r\|_\infty}{\|E_h\|_\infty}$ at $t = 6$ ns

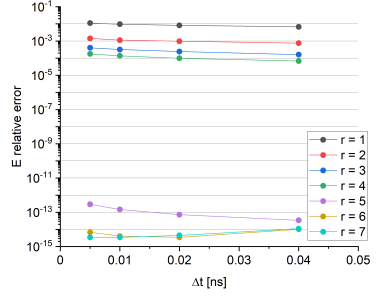
Figure 6: Results of time step refinement the MLQD method with the MBE-SC scheme and POD of the intensity $\Delta x = 6 \times 10^{-2}$ cm.



(a) $\frac{\|E_h - E_h^r\|_\infty}{\|E_h\|_\infty}$ at $t = 0.4$ ns



(b) $\frac{\|E_h - E_h^r\|_\infty}{\|E_h\|_\infty}$ at $t = 1$ ns



(c) $\frac{\|E_h - E_h^r\|_\infty}{\|E_h\|_\infty}$ at $t = 6$ ns

Figure 7: Results of time step refinement the MLQD method with the MBE-SC scheme and POD of the remainder term for $\Delta x = 6 \times 10^{-2}$ cm.

References

- [1] V. Ya. Gol'din, G. V. Danilova, B. N. Chetverushkin, Approximate method for solving time-dependent kinetic equation, in: Computational Methods in Transport Theory, Atomizdat, Moscow, 1969, pp. 50–57, (in Russian).
- [2] A. Matsekh , L. Chacon, H. Park, G. Chen, Machine learning for memory reduction in the implicit monte carlo simulations of thermal radiative transfer, Tech. Rep. LA-UR-18-25444, Los Alamos National Laboratory (2018).
- [3] Z. Peng, R. G. McClarren, M. Frank, A low-rank method for time-dependent transport calculations, in: Proc. of Int. Conf. on Math. and Comp., M&C 2019, Portland, OR, USA, 2019, pp. 957–965.
- [4] P. Ghassemi, D. Y. Anistratov, An approximation method for time-dependent problems in high energy density thermal radiative transfer, Journal of Computational and Theoretical Transport 41 (2020) 31–50.
- [5] D. Y. Anistratov, Implicit methods with reduced memory for time-dependent boltzmann transport equation, Transactions of American Nuclear Society 122 (2020) 367–370.
- [6] D. Y. Anistratov, E. N. Aristova, V. Y. Gol'din, A nonlinear method for solving problems of radiation transfer in a physical system, Mathematical Modeling 8 (1996) 3–28, in Russian.
- [7] D. Y. Anistratov, Stability analysis of a multilevel quasidiffusion method for thermal radiative transfer problems, Journal of Computational Physics 376 (2019) 186–209.
- [8] L. Sirovich, Turbulence and the dynamics of coherent structures. parts i-iii, Quarterly of Applied Mathematics XLV (1987) 561–590.
- [9] G. Berkooz, P. Holmes, J. L. Lumley, The proper orthogonal decomposition in the analysis of turbulent flows, Annual Review of Fluid Mechanics 25 (1993) 539–575.
- [10] K. Kunisch, S. Volkwein, Galerkin proper orthogonal decomposition methods for a general equation in fluid dynamics, SIAM J. Numer. Anal 40 (2002) 492–515.
- [11] V. Ya. Gol'din, A quasi-diffusion method of solving the kinetic equation, USSR Comp. Math. and Math. Phys. 4 (1964) 136–149.
- [12] V. Ya. Gol'din, B. N. Chetverushkin, Methods of solving one-dimensional problems of radiation gas dynamics, USSR Comp. Math. and Math. Phys. 12 (1972) 177–189.
- [13] L. H. Auer, D. Mihalas, On the use of variable Eddington factors in non-LTE stellar atmospheres computations, Monthly Notices of the Royal Astronomical Society 149 (1970) 65–74.
- [14] I. Ipsen, Numerical Matrix Analysis, SIAM, Philadelphia, PA, 2009.
- [15] J. A. Fleck, J. D. Cummings, An implicit monte carlo scheme for calculating time and frequency dependent nonlinear radiation transport, Journal of Computational Physics 8 (1971) 313–342.